# LISA observations of rapidly spinning massive black hole binary systems

Alberto Vecchio
*School of Physics and Astronomy, The University of Birmingham, Edgbaston, Birmingham B15 2TT, UK*
(Dated: February 2, 2008)

Binary systems of massive black holes will be detectable by the Laser Interferometer Space Antenna (LISA) throughout the entire Universe. Observations of gravitational waves from this class of sources will have important repercussions on our understanding of the behaviour of gravity in the highly non-linear relativistic regime, the distribution and interaction of massive black holes at high redshift and the formation and evolution of cosmic structures. It is therefore important to address how accurately LISA can measure the source parameters and explore the implications for astronomy and cosmology.

Present observations and theoretical models suggest that massive black holes could be spinning, possibly rapidly in some cases. In binary systems, the relativistic spin-orbit interaction causes the orbital plane to precess in space producing a characteristic signature on the emitted gravitational waves. In this paper we investigate the effect of spins on the gravitational wave signal registered at the LISA output – we provide ready-to-use analytical expressions of the measured signal – and the implications for parameter estimation. We consider the in-spiral phase of binary systems in circular orbit undergoing the so-called "simple precession" and we approximate the gravitational radiation at the restricted post$^{1.5}$-Newtonian order. We show that the presence of spins changes dramatically the signature of the signal recorded by LISA. As a consequence, the mean square errors associated to the parameter measurements are significantly smaller than the ones obtained when the effect of spins is neglected. For a binary system of two $10^6\,M_\odot$ black holes, the angular resolution and the relative error on the luminosity distance improve by a factor $\approx$ 3-to-10; the fractional errors on the chirp mass and the reduced mass decrease by a factor $\sim 10$ and $\sim 10^3$, respectively.



## I. INTRODUCTION

Binary systems of massive black holes in the mass range $10^7\,M_\odot - 10^5\,M_\odot$ are among the most spectacular sources that will be observed by the Laser Interferometer Space Antenna (LISA), an ESA/NASA space-borne laser interferometer aimed at observations of gravitational waves (GW's) in the low-frequency region of the spectrum $\sim 10^{-5}$ Hz - 0.1 Hz, and expected to be launched in 2011 [1]. The interest in the detection of gravitational radiation from massive black holes (MBH's) is two-fold [2]: (i) for fundamental physics, because it will provide a thorough understanding of the behaviour of strong gravity in the highly non-linear relativistic regime, and (ii) for astronomy and cosmology because GW's provide an "orthogonal" and complementary mean, with respect to conventional astronomy, of investigating the high-redshift formation and evolution of cosmic structures, such as galaxy interactions and mergers, and exploring the demography of massive black holes.

Massive black holes (MBH's) are considered to be essentially ubiquitous in the centre of galaxies in the local and low-redshift Universe [3, 4]. Our Galaxy [5] and NGC 4258 [6] provide probably the most solid observational evidence for the existence of such black holes [7]. The evidence for the presence of black holes in galaxies at high redshift is more circumstantial, but the fact that galaxies, at some stage of their life, harbour AGN's, and we observe quasars at $z \gtrsim 6$ [8] strongly favour the hypothesis that black holes are fairly common also at high redshift. This conclusion is supported by recent results [9] that show that the high-redshift quasar distribution and the present day density of black holes can be reconciled by invoking galaxy mergers where the relation between host velocity dispersion and black hole mass is consistent with the one observed locally [10]. The present day population of MBH's is therefore likely to be the dormant remnant of those earlier activities. Two black holes are brought together at the centre of a merger remnant by dynamical friction from the stars of the common host. The further evolution of a binary must then take place on a time scale short enough for the system to coalesce within an Hubble time due to radiation reaction. Two are the main mechanisms that could make the binary hard enough to satisfy this condition: dynamical friction from stars in the core [11, 12, 13, 14, 15] and gas dynamical effects [16, 17]. However, despite all these circumstantial evidences, the rate of coalescence of massive black hole binaries in the Universe is still controversial: present astrophysical estimations vary widely from $\sim 0.1\,\mathrm{yr}^{-1}$ to $\sim 100\,\mathrm{yr}^{-1}$ [11, 18, 19, 20, 21, 22, 23, 24], depending on model assumptions and BH mass range. At present there are no direct observational evidences for the presence of massive black holes binary systems, with the possible exception of OJ287 [25].

LISA will be able to detect MBH binaries at a moderate-to-high signal-to-noise ratio throughout the entire Universe (redshift $z \approx 10$ and beyond, if black holes are already present). During the whole LISA observational campaign – the nominal duration of the mission is 3 years, but the instrument is expected to operate for about 10 years, if no catastrophic failure occurs on the spacecraft – one can therefore expect from a handful to a very large number of

detections.

LISA is an all-sky monitor. At any one time, the instrument maps the whole sky, although with a different sensitivity depending on the location of the source and the polarisation of the waves. By coherently tracking the phase and amplitude evolution of GW's, one can extract precise information about a source. In observations of binary systems, the number of parameters on which the waveform depends, and that one needs to extract from the data, is large, in the most general case 17. Clearly correlations among parameters are inevitable, degrading the precision of the measurements.

A few studies have been carried out so far to address how accurately LISA can measure the source parameters and the implications for astronomy and cosmology. Because of the complexity of the problem and open theoretical issues in the modelling of the gravitational waveform in the most general case, assumptions, possibly ad-hoc, have been introduced on the waveform model. Cutler [26] has considered the in-spiral phase of binary systems approximating the waveform at the restricted post$^{1.5}$-Newtonian order. Sintes and collaborators [27, 28] and Moore and Hellings [29] have investigated the parameter estimation including post$^{2}$-Newtonian corrections to the amplitude and the phase. Hughes [30] has considered restricted post$^{2}$-Newtonian waveforms for the in-spiral phase and has included the ring-down portion of the signal; more recently Seto has included the effect of the finite length of the LISA arms using restricted post$^{1.5}$-Newtonian waveforms [31]. All these analysis have *a priori* assumed that black holes have no spins, or the spins are parallel to each other and the orbital angular momentum. However, present astrophysical observations and theoretical models suggest that massive black holes are likely to be rotating, possibly rapidly in some cases. Observations of AGN's and quasars are highly consistent with rapidly rotating black holes; observations of black holes in quiescence are in agreement with a slow, if any, rotation and some theoretical models suggest small-to-moderate spins (see, *e.g.*, [32]). If there is little doubt that black holes are, in general, rotating, how strong spins are is to a large extent unknown. Quite likely, gravitational wave observations shall provide the most effective tool in addressing this issue. Spins are likely to add vast complexity to the signal recorded at the detector output, and require more parameters to describe the waveform [33, 34, 35, 36]. In this paper we show that spins do change dramatically the structure of the signal observed by LISA and, as a consequence, affect significantly (even by orders of magnitudes for some selected parameters) the errors with which LISA can measure the source parameters.

In this paper we restrict our attention to the in-spiral phase of massive binary systems of comparable mass. We consider circular orbits, model the waveform at the restricted post$^{1.5}$-Newtonian order and assume that binary systems undergo the so-called *simple precession* [33], which is the relevant scenario from an astrophysical viewpoint. The goal of the paper is two fold: (i) to provide ready to use analytical expressions for the LISA detector output when binary systems undergo spin-orbit precession, and (ii) to show the dramatic change in parameter estimation that occurs when spin-orbit modulation in phase and amplitude is taken into account. The actual parameter space is so vast – the waveform is described by 12 parameters – that here we concentrate on typical systems of two $10^6\,M_\odot$ black holes. A thorough exploration of the whole parameter space requires large-scale, CPU-intensive Monte-Carlo simulations and is beyond the scope of this paper; such analysis is currently in progress and will be reported in a separate paper [37].

The organisation of the paper is as follows. In section II we review the main features of the LISA mission, in particular its orbital configuration which is central for the topic discussed in this paper. In Section III we review the main properties and key equations regarding the emission of GW's from in-spiralling binary systems, with emphasis on the role plaid by spins, and we stress the differences with respect to the non-spinning, i.e. non-precessing, case. Section IV and V contain the key results of the paper. In Section IV we derive explicit ready-to-use analytical expressions for the signal measured at the LISA detector output for binary systems in circular orbit that undergo simple precession; the waveform is computed within the restricted post$^{1.5}$-Newtonian approximation. In section V we explore the errors with which the twelve parameters of the signal can be determined and compare the results with the case where spins are neglected. In Section VI we summarise our conclusions and present pointers to future work.

## II. THE LISA MISSION

In this section we review the main properties of the LISA mission. We refer the reader to [1] for more details.

### A. The LISA orbit

LISA is an all-sky monitor with a quadrupolar antenna pattern. Its orbital configuration is conceived in order to keep the geometry of the interferometer as stable as possible during the mission, which in turn provides a thorough coverage of the whole sky: a constellation of three drag-free spacecraft (containing the "free-falling test masses") is placed at the vertexes of an ideal equilateral triangle with sides $\simeq 5\times10^6\,$km; it forms a three-arms interferometer, with a $60^\circ$ angle between two adjacent laser beams. The LISA orbital motion is as follows: the barycentre of the

instrument follows an essentially circular heliocentric orbit, 20° behind the Earth; the detector plane is tilted by 60° with respect to the Ecliptic and the instrument counter-rotates around the normal to the detector plane with the same period 1 yr.

Following [26] we introduce two Cartesian reference frames [38]: (i) a fixed "barycentric" frame $(x, y, z)$ tied to the Ecliptic and centred in the Solar System Barycentre, with $\hat{\mathbf{z}}$ perpendicular to the Ecliptic, and the plane $(x, y)$ in the Ecliptic itself; (ii) a detector reference frame $(x', y', z')$, centred in the LISA centre of mass and attached to the detector, with $\hat{\mathbf{z}}'$ perpendicular to the plane defined by the three arms and the $x'$ and $y'$ axis defined so that the unit vectors $\hat{\mathbf{l}}_j$ $(j = 1, 2, 3)$ along each arm read

$$\hat{\mathbf{l}}_j = \cos\left[\frac{\pi}{12} + \frac{\pi}{3}(j-1)\right]\hat{\mathbf{x}}' + \sin\left[\frac{\pi}{12} + \frac{\pi}{3}(j-1)\right]\hat{\mathbf{y}}' \,. \tag{1}$$

In the Ecliptic frame the motion of LISA's centre-of-mass is described by the polar angles

$$\begin{aligned} \Theta &= \frac{\pi}{2}\,, \\ \Phi(t) &= \Phi_0 + n_\oplus t\,, \end{aligned} \tag{2}$$

where

$$n_\oplus \equiv \frac{2\pi}{1\,\mathrm{yr}}\,, \tag{3}$$

and $\Phi_0$ sets the position of the detector at same arbitrary reference time. The normal to the detector plane $\hat{\mathbf{z}}'$ precesses around $\hat{\mathbf{z}}$ according to

$$\hat{\mathbf{z}}' = \frac{1}{2}\hat{\mathbf{z}} - \frac{\sqrt{3}}{2}\left[\cos\Phi(t)\hat{\mathbf{x}} + \sin\Phi(t)\hat{\mathbf{y}}\right] \,. \tag{4}$$

The time evolution of the unit vectors $\hat{\mathbf{l}}_j$ $(j = 1, 2, 3)$ along each arm is described by the following expression [26]:

$$\begin{aligned} \hat{\mathbf{l}}_j = & \left[\frac{1}{2}\sin\alpha_j(t)\,\cos\Phi(t) - \cos\alpha_j(t)\,\sin\Phi(t)\right]\hat{\mathbf{x}} \\ & + \left[\frac{1}{2}\sin\alpha_j(t)\,\sin\Phi(t) + \cos\alpha_j(t)\,\cos\Phi(t)\right]\hat{\mathbf{y}} + \left[\frac{\sqrt{3}}{2}\sin\alpha_j(t)\right]\hat{\mathbf{z}}\,, \end{aligned} \tag{5}$$

where $\alpha_j(t)$ increases linearly with time, according to

$$\alpha_j(t) = n_\oplus t - (j-1)\pi/3 + \alpha_0 \,, \tag{6}$$

and $\alpha_0$ is just a constant specifying the orientation of the arms at the arbitrary reference time $t = 0$.

### B. The LISA detector output

The strain $h(t)$ produced at the output of the LISA Michelson interferometer by a GW signal characterised by the two independent polarisation states $h_+(t)$ and $h_\times(t)$ [42] is

$$h^{(\iota)}(t) = \frac{\sqrt{3}}{2}\left[F_+^{(\iota)}(t)h_+(t) + F_\times^{(\iota)}(t)h_\times(t)\right] \,. \tag{7}$$

In Eq. (7) $F_+^{(\iota)}(t)$ and $F_\times^{(\iota)}(t)$ are the *time dependent* antenna patters and the factor $\sqrt{3}/2 = \sin(\pi/3)$ comes from the 60° opening angle of the LISA arms. $F_+$ and $F_\times$ vary with time because during the observation the interferometer changes orientation with respect to the source; in fact, in-spiral binaries are long-lived sources in the low frequency band. The index $\iota = I, II$ labels the two independent Michelson outputs that can be constructed from the readouts of the three arms if the noise is uncorrelated and "totally symmetric" [26]. They are equivalent to the outputs of two identical interferometers in the same location, rotated by 45° one with respect to the other.

The functions describing the interferometer beam pattern depend on the source location in the sky $\hat{\mathbf{N}}$ (GW's propagate in the $-\hat{\mathbf{N}}$ direction) and wave polarisation, which is related to the orientation of the orbital plane, and therefore the orbital angular momentum $\hat{\mathbf{L}}$, with respect to the detector. With respect to the frame tied to the Solar

system barycentre, $\hat{\mathbf{N}}$ and $\hat{\mathbf{L}}$ are described by the polar angles $(\theta_N\,,\phi_N)$ and $(\theta_L\,,\phi_L)$. Equivalently, in the frame attached to the detector, $\hat{\mathbf{N}}$ and $\hat{\mathbf{L}}$ are identified by the angles $(\theta'_N\,,\phi'_N)$ and $(\theta'_L\,,\phi'_L)$. In the reference frame attached to LISA, the antenna beam patters read

$$F_+\left(\theta'_N\,,\phi'_N\,\psi'_N\right)=\frac{1}{2}(1+\cos\theta'^2_N)\cos 2\phi'_N\cos 2\psi'_N-\cos\theta'_N\sin 2\phi'_N\sin 2\psi'_N\,, \tag{8a}$$

$$F_\times\left(\theta'_N\,,\phi'_N\,\psi'_N\right)=\frac{1}{2}(1+\cos\theta'^2_N)\cos 2\phi'_N\sin 2\psi'_N+\cos\theta'_N\sin 2\phi'_N\cos 2\psi'_N\,, \tag{8b}$$

where $\psi'_N$ describes the "polarisation angle" of the waveform in the detector frame. The antenna patterns (8a) and (8b) for the two outputs $\iota=I$ and $\iota=II$ are therefore

$$F^{(\iota)}_{+,\times}(t)\;=\;\begin{cases}F_{+,\times}\left(\theta'_N\,,\phi'_N\,\psi'_N\right) & (\iota=I)\\ F_{+,\times}\left(\theta'_N\,,(\phi'_N-\pi/4)\,,\psi'_N\right) & (\iota=II)\end{cases}\,. \tag{9}$$

Note that because of the detector change of orientation, the angles $\theta'_N$, $\phi'_N$ and $\psi'_N$ are time dependent. As a function of the angles measured in the Solar System Barycentre they read

$$\cos\theta'_N(t)\;=\;\frac{1}{2}\cos\theta_N-\frac{\sqrt{3}}{2}\sin\theta_N\cos(\Phi(t)-\phi_N)\,, \tag{10}$$

$$\phi'_N(t)\;=\;\Xi_1+\frac{\pi}{12}+\tan^{-1}\left\{\frac{\frac{\sqrt{3}}{2}\cos\theta_N+\frac{1}{2}\sin\theta_N\sin(\Phi(t)-\phi_N)}{\sin\theta_N\sin(\Phi(t)-\phi_N)}\right\}\,, \tag{11}$$

$$\tan\psi'_N\;=\;\frac{\hat{\mathbf{L}}\cdot\hat{\mathbf{z}}'-(\hat{\mathbf{L}}\cdot\hat{\mathbf{N}})\,(\hat{\mathbf{z}}'\cdot\hat{\mathbf{N}})}{\hat{\mathbf{N}}\cdot(\hat{\mathbf{L}}\times\hat{\mathbf{z}}')}\,, \tag{12}$$

where

$$\Xi_j=n_\oplus t-\frac{\pi}{12}-\frac{\pi}{3}(j-1)+\Xi_0\,, \tag{13}$$

and $\Xi_0$ sets the orientation of $\hat{\mathbf{l}}_j$ at $t=0$. We are not yet ready to derive the explicit expression for $\psi'_N$, Eq.(12), because for spinning black holes, the source at the centre of this paper, $\hat{\mathbf{L}}$ is not a constant of motion. We derive the necessary equations in the following section.

## III. GRAVITATIONAL WAVES FROM BINARY SYSTEMS

In this section we briefly review, partly to fix notation, the basic concepts and formulae regarding the emission of gravitational waves by binary systems, with emphasis on the effects produced by spins. We refer the reader to [33, 34] for details and to [39] and references therein for a thorough review regarding post-Newtonian gravitational waveforms.

The whole *coalescence* of a binary system is usually divided in three distinct phases [40]: (i) the adiabatic in-spiral, during which the BH orbital evolution occurs on the time-scale of the gravitational radiation reaction, which is much longer than the orbital period; (ii) the merger, which takes place at the end of the in-spiral when the binary orbit becomes relativistically unstable and the black holes enter a free fall plunge; and (iii) the ring-down, when the resulting BH settles down in its final stationary Kerr state, oscillating according to its normal modes. In this paper we consider only the in-spiral phase. In fact the time to coalescence for a system radiating at frequency $f$ is:

$$\tau\simeq 1.2\times 10^7\left(\frac{f}{10^{-4}\,\mathrm{Hz}}\right)^{-8/3}\left(\frac{M\,(1+z)}{10^6\,M_\odot}\right)^{-5/3}\left(\frac{\eta}{0.25}\right)^{-1}\,\mathrm{sec}\,, \tag{14}$$

where $M$ and $\eta$ are the total mass and the symmetric mass ratio, respectively, defined in Eqs. (16b)-(16e), $\tau$ is the *observed* life-time of a binary system as recorded in the solar system for a source at redshift $z$ with intrinsic total mass $M$ that enters the detector window at the observed frequency $f=10^{-4}$ Hz. Binary systems are therefore long-lived in the LISA band, and one critically relies on long integration times to disentangle the sources parameters, in particular to resolve the source position in the sky and measure its luminosity distance [26].

As we consider only the in-spiral phase of the coalescence, in the frequency domain we shut-off the signal at frequency

$$f_{\rm isco} = \frac{1}{\pi\, 6^{3/2} M\,(1+z)} \simeq 4.4\times 10^{-3}\left(\frac{M\,(1+z)}{10^6\,M_\odot}\right)^{-1}\,{\rm Hz}\,, \tag{15}$$

which corresponds to the innermost stable circular orbit of a particle orbiting a Schwarzichild black hole (ISCO). The real transition from in-spiral to merger will occur at a frequency somewhat (by a factor $\lesssim 2$) different from $f_{\rm isco}$, but due to the difficulty of defining the ISCO we will adopt the value (15). The results presented in this paper are anyway essentially unaffected by changing the cut-off frequency by a small factor.

We also assume the orbit to be circular. This is completely reasonable from an astrophysical point of view, as a massive binary system of roughly equal mass black holes has enough time – regardless of the initial eccentricity at which it forms – to circularise before it enters the observational window, due to dynamical friction and radiation reaction [12, 41].

### A. The amplitude and phase evolution

We consider two massive black holes of mass $m_1$ and $m_2$, and spins $\mathbf{S}_1$ and $\mathbf{S}_2$, respectively. Several mass parameters are actually useful:

$$M = m_1 + m_2\,, \tag{16a}$$
$$\mu = \frac{m_1\, m_2}{M}\,, \tag{16b}$$
$$\mathcal{M} = \mu^{3/5}\, M^{2/5} = M\,\eta^{3/5}\,, \tag{16c}$$
$$\eta = = \frac{\mu}{M}\,; \tag{16d}$$
$$\tag{16e}$$

they represent, respectively, the total mass, the reduced mass, the chirp mass and the symmetric mass ratio.

The system evolves by loosing energy and angular momentum through emission of gravitational waves of increasing frequency and amplitude. The emitted radiation is given by the superposition of harmonics at multiples of the orbital period, and the two independent polarisation amplitudes $h_+$ and $h_\times$ [42] can be schematically represented as [43]

$$h_{+,\times}(t) = \Re\left\{\sum_k H^{(k)}_{+,\times}(t)\, e^{i\,k\,\phi_{\rm orb}(t)}\right\}\,, \tag{17}$$

where $H^{(k)}_{+,\times}$ are time dependent functions of the source parameters and $\phi_{\rm orb}(t)$ is the binary orbital phase. The strongest harmonic is associated to the quadrupole moment of the source, and therefore corresponds to $k=2$. In this paper we consider the so-called *restricted post-Newtonian approximation* to the radiation (17): we retain only the leading order contribution to the amplitude, therefore only $H^{(2)}_{+,\times}$ at the Newtonian order, and take into account post-Newtonian corrections only to the phase of the signal $\phi(t) = 2\,\phi_{\rm orb}(t)$. In this approximation Eq. (17) reads:

$$h_+ = 2\frac{\mathcal{M}^{5/3}}{D_L}\left[1+\left(\hat{\mathbf{L}}\cdot\hat{\mathbf{N}}\right)^2\right](\pi\, f)^{2/3}\,\cos\phi(t)\,, \tag{18a}$$
$$h_\times = -4\frac{\mathcal{M}^{5/3}}{D_L}\left(\hat{\mathbf{L}}\cdot\hat{\mathbf{N}}\right)(\pi\, f)^{2/3}\sin\phi(t)\,, \tag{18b}$$

where $D_L$ is the source luminosity distance [44], $\hat{\mathbf{N}}$ the unit vector pointing toward the binary centre of mass (in our convention the GW propagation direction is $-\hat{\mathbf{N}}$) and $\hat{\mathbf{L}}$ the orbital angular momentum unit vector.

We review now the expression for the GW phase $\phi(t)$. The signal frequency $f$, twice the orbital one, evolves according to [45]

$$\frac{df}{dt} = \frac{96}{5}\,\pi^{8/3}\,\mathcal{M}^{5/3}\,f^{11/3}\Bigg[1-\left(\frac{743}{336}+\frac{11}{4}\eta\right)(\pi M f)^{2/3} + (4\pi-\beta)(\pi M f) + \left(\frac{34103}{18144}+\frac{13661}{2016}\eta+\frac{59}{18}\eta^2+\sigma\right)(\pi M f)^{4/3}\Bigg]\,, \tag{19}$$

where Eq. (19) is valid through the post$^2$-Newtonian order and

$$\beta = \frac{1}{12}\sum_{i=1}^{2}\left[113\left(\frac{m_i}{M}\right)^2+75\eta\right]\left(\hat{\mathbf{L}}\cdot\frac{\mathbf{S}_i}{m_i^2}\right), \tag{20}$$

$$\sigma = \frac{\eta}{48}\left\{-247\left(\frac{\mathbf{S}_1}{m_1^2}\cdot\frac{\mathbf{S}_2}{m_2^2}\right)+721\left[\hat{\mathbf{L}}\cdot\frac{\mathbf{S}_1}{m_1^2}\right]\left[\hat{\mathbf{L}}\cdot\frac{\mathbf{S}_1}{m_1^2}\right]\right\} \tag{21}$$

are the so called *spin-orbit* and *spin-spin parameters*, respectively [45]. From Eq. (19) and $d\phi/dt = 2\pi f$, one can derive the time and phase evolution of the gravitational radiation:

$$t(f) = t_c - 5\,(8\pi f)^{-8/3}\,\mathcal{M}^{-5/3}\left[1+\frac{4}{3}\left(\frac{743}{336}+\frac{11}{4}\eta\right)(\pi Mf)^{2/3}-\frac{8}{5}\,(4\pi-\beta)\,(\pi Mf)\right.$$
$$\left.+\,2\left(\frac{3058673}{1016064}+\frac{5429}{1008}\,\eta+\frac{617}{144}\,\eta^2-\sigma\right)(\pi Mf)^{4/3}\right], \tag{22}$$

$$\phi(f) = \phi_c - \frac{1}{16}\,(\pi f\mathcal{M})^{-5/3}\left[1+\frac{5}{3}\left(\frac{743}{336}+\frac{11}{4}\eta\right)(\pi Mf)^{2/3}-\frac{5}{2}\,(4\pi-\beta)\,(\pi Mf)\right.$$
$$\left.+\,5\left(\frac{3058673}{1016064}+\frac{5429}{1008}\,\eta+\frac{617}{144}\,\eta^2-\sigma\right)(\pi Mf)^{4/3}\right]; \tag{23}$$

$t_c$ and $\phi_c$, the *time* and *phase at coalescence*, are constants of integration, defined as the value of $t$ and $\phi$ at (formally) $f=\infty$. As we mentioned, massive black holes spend months-to-years in the LISA observational window, depending on the mass. For future reference, if we assume that LISA observes the final year of in-spiral of a binary, then the signal sweeps the frequency band between

$$f_{\rm a} \simeq 4.2\times10^{-5}\left(\frac{T_{\rm obs}}{1\,{\rm yr}}\right)^{-3/8}\left[\frac{\mathcal{M}\,(1+z)}{10^6\,M_\odot}\right]^{-5/8}, \tag{24}$$

which we call "arrival" (or "initial") frequency, and $f_{\rm isco}$. An interesting quantity to consider is the total number of gravitational wave cycles recorded by the detector:

$$\mathcal{N}(t) = \frac{1}{2\pi}\int_{t_a}^{t}\phi(t')\,dt'\,. \tag{25}$$

From Eq. (23) and (24), it is easy to compute the number of cycles in the final year of in-spiral:

$$\mathcal{N} \approx 4.8\times10^2\left(\frac{f_{\rm a}}{10^{-4}\,{\rm Hz}}\right)^{-5/3}\left[\frac{\mathcal{M}\,(1+z)}{10^6\,M_\odot}\right]^{-5/3}$$
$$\approx 2.1\times10^3\left(\frac{T_{\rm obs}}{1\,{\rm yr}}\right)^{5/8}\left[\frac{\mathcal{M}\,(1+z)}{10^6\,M_\odot}\right]^{-5/8}. \tag{26}$$

Table I contains reference values for $f_{\rm a}$, $f_{\rm isco}$ and $\mathcal{N}$ for a number of choices of masses and observation times.

### B. Spin induced precession

Present observations and theoretical prejudices suggest that massive black holes could be rapidly rotating. As we have mentioned in the previous section, if black holes are spinning then the GW phase (23) contains two additional terms, one at the 1.5PN order, which is proportional to $\beta$, and the other at the 2PN order, which is proportional to $\sigma$. However spins introduce a much more dramatic effect in the structure of the waveform, which is qualitatively different from the ones just mentioned: the orbital angular momentum $\mathbf{L}$ and the spins $\mathbf{S}_1$ and $\mathbf{S_2}$ change orientation due to spin-orbit interaction (1.5PN effect), so that the radiation detected has a time varying polarisation. $\mathbf{L}$, $\mathbf{S}_1$ and $\mathbf{S_2}$ precess, over a time scale longer than the orbital period ($2/f \sim 30$ min) but shorter than the observation time ($\sim 1$ yr), around the (almost) fixed direction of the total angular momentum $\mathbf{L}+\mathbf{S}_1+\mathbf{S_2}$. This effect is actually quite dramatic and drastically changes the signature of the detected signal, as the orientation of the orbital plane changes

TABLE I: Summary of the frequency band swept by massive black hole binary systems and the number of wave cycles recorded at the detector output in LISA observations for selected masses and integration times. The table shows the initial and final frequency of the GW's, $f_{\rm a}$ and $f_{\rm isco}$ respectively, the corresponding time of observation $T_{\rm obs}$, and the number of waves cycles recored at the output of the detector, coming from the various contributions of the terms in Eq. (23): Newtonian: the first term; post$^1$-Newtonian (1PN): the second term, proportional to $(\pi\,M\,f)^{2/3}$; tail: $-10\,\pi\,(\pi\,M\,f)$; spin-orbit: $(5/2)\,\beta\,(\pi\,M\,f)$; post$^2$-Newtonian (2PN): the last term, proportional to $(\pi\,M\,f)^{4/3}$ with $\sigma = 0$; spin-spin: the $-5\,\sigma\,(\pi\,M\,f)^{4/3}$ term. The sources are selected with masses in the range $10^7\,M_\odot$ - $10^5\,M_\odot$; for each mass choice, three different $f_{\rm a}$'s are considered: the first corresponds to $T_{\rm obs}$ =1 yr, which does depend on $m_1$ and $m_2$, whereas the other two are the same for all $m_1$ and $m_2$, and correspond to $f_{\rm a} = 5\times10^{-5}$ Hz , and $10^{-4}$ Hz, respectively. Notice that depending on $f_{\rm a}$, $m_1$ and $m_2$, systems are observable for different times. The fiducial source is at $z = 1$.

| | | | | | number of wave cycles | | | | | |
|---|---|---|---|---|---|---|---|---|---|---|
| $m_1$ | $m_2$ | $f_a$ | $f_{\rm isco}$ | $T_{\rm obs}$ | Newt. | 1PN | tail | spin-orbit | 2PN | spin-spin |
| ($M_\odot$) | ($M_\odot$) | ($\times10^{-4}$ Hz) | ($\times10^{-4}$ Hz) | (yr) | | | | ($\times\beta$) | | ($\times\sigma$) |
| $10^7$ | $10^7$ | 0.070 | 1.099 | 1.000 | 342 | 42 | -40 | 3 | 3 | -1 |
| $10^7$ | $10^7$ | 0.500 | 1.099 | 0.004 | 10 | 3 | -5 | 0 | 1 | 0 |
| $10^7$ | $10^6$ | 0.153 | 1.999 | 1.000 | 761 | 87 | -103 | 8 | 7 | -2 |
| $10^7$ | $10^6$ | 0.500 | 1.999 | 0.038 | 96 | 22 | -34 | 3 | 3 | -1 |
| $10^7$ | $10^6$ | 1.000 | 1.999 | 0.005 | 23 | 7 | -13 | 1 | 1 | 0 |
| $10^7$ | $10^5$ | 0.350 | 2.177 | 1.000 | 1792 | 290 | -455 | 36 | 32 | -10 |
| $10^7$ | $10^5$ | 0.500 | 2.177 | 0.366 | 949 | 187 | -319 | 25 | 24 | -8 |
| $10^7$ | $10^5$ | 1.000 | 2.177 | 0.045 | 238 | 65 | -130 | 10 | 11 | -4 |
| $10^7$ | $10^4$ | 0.776 | 2.196 | 1.000 | 4102 | 990 | -1881 | 150 | 153 | -51 |
| $10^7$ | $10^4$ | 0.500 | 2.196 | 3.649 | 9477 | 1834 | -3160 | 252 | 235 | -78 |
| $10^7$ | $10^4$ | 1.000 | 2.196 | 0.447 | 2383 | 647 | -1296 | 103 | 110 | -37 |
| $10^6$ | $10^6$ | 0.295 | 10.993 | 1.000 | 1453 | 102 | -76 | 6 | 5 | -1 |
| $10^6$ | $10^6$ | 0.500 | 10.993 | 0.246 | 602 | 59 | -51 | 4 | 4 | -1 |
| $10^6$ | $10^6$ | 1.000 | 10.993 | 0.038 | 187 | 28 | -30 | 2 | 3 | -1 |
| $10^6$ | $10^5$ | 0.647 | 19.987 | 1.000 | 3216 | 215 | -201 | 16 | 11 | -3 |
| $10^6$ | $10^5$ | 0.500 | 19.987 | 1.991 | 4950 | 280 | -243 | 19 | 12 | -4 |
| $10^6$ | $10^5$ | 1.000 | 19.987 | 0.312 | 1552 | 137 | -144 | 11 | 9 | -3 |
| $10^6$ | $10^4$ | 1.508 | 21.768 | 1.000 | 7571 | 748 | -943 | 75 | 55 | -18 |
| $10^6$ | $10^4$ | 0.500 | 21.768 | 19.285 | 48121 | 2366 | -2176 | 173 | 96 | -31 |
| $10^6$ | $10^4$ | 1.000 | 21.768 | 3.019 | 15096 | 1155 | -1300 | 103 | 68 | -22 |
| $10^5$ | $10^5$ | 1.242 | 109.929 | 1.000 | 6161 | 247 | -141 | 11 | 8 | -2 |
| $10^5$ | $10^5$ | 0.500 | 109.929 | 11.261 | 28097 | 618 | -266 | 21 | 11 | -2 |
| $10^5$ | $10^5$ | 1.000 | 109.929 | 1.781 | 8848 | 308 | -165 | 13 | 9 | -2 |
| $10^5$ | $10^4$ | 2.729 | 199.872 | 1.000 | 13594 | 519 | -374 | 30 | 16 | -5 |
| $10^5$ | $10^4$ | 0.500 | 199.872 | 91.802 | 230221 | 2867 | -1208 | 96 | 33 | -9 |
| $10^5$ | $10^4$ | 1.000 | 199.872 | 14.494 | 72508 | 1430 | -753 | 60 | 25 | -7 |

during the year long observation time, and the angular momenta complete several precession cycles around the fixed detection.

The spin-orbit induced precession is the key new physical effect which is introduced in this paper. Here we review the main concepts and expressions and refer the reader to [33, 34] for more details. In this paper we restrict our attention to the so-called *simple precession* [33], which takes place when (i) the BH masses are equal ($m_1 \sim m_2$), *or* (ii) one of the BH's has negligible spin (for convention, in this paper we shall assume $S_2 = 0$). Furthermore, one needs to impose the condition that the angular momenta are oriented so that $\mathbf{L} \neq -(\mathbf{S_1} + \mathbf{S_2})$. Under this assumptions the equations that describe the evolution of the angular momenta simplify considerably, and one can construct explicit analytical solutions for the relevant quantities. Moreover the regime that we consider is well justified form an astrophysical point of view.

For circular orbits through the post$^{1.5}$-Newtonian order the equations describing the evolution of $\mathbf{L}$, $\mathbf{S}_1$ and $\mathbf{S_2}$ read

$$\dot{\hat{\mathbf{L}}} = \left[\frac{1}{r^3}\left(2+\frac{3m_2}{2m_1}\right)\mathbf{J}\right]\times\hat{\mathbf{L}}\,, \tag{27}$$

$$\dot{\hat{S}} = \left[\frac{1}{a^3}\left(2+\frac{3m_2}{2m_1}\right)\mathbf{J}\right]\times\hat{\mathbf{S}}\,, \tag{28}$$

$$\frac{d}{dt}\left(\mathbf{S}_1\cdot\mathbf{S}_2\right) = 0\,, \tag{29}$$

$$\dot{S} = 0\,, \tag{30}$$

where

$$\mathbf{J} = \mathbf{L} + \mathbf{S} \qquad (\mathbf{S} = \mathbf{S_1} + \mathbf{S_2}) \tag{31}$$

is the conserved total angular momentum [46, 47] (indeed $\dot{\mathbf{L}} = -\dot{\mathbf{S}}$).

Following [33], we highlight the main features of simple precession and provide, in a ready-to-use form, the relevant quantities needed for the computation of the LISA detector output. We will neglect the post$^2$-Newtonian corrections, while retaining the post$^{1.5}$-Newtonian terms (spin-orbit), which are dominant, for the $m_1 = m_2$ case; they vanish anyway for $S_2 = 0$ [33, 34].

One can summarise the main features of the *simple precession* as follows. $\hat{\mathbf{J}}$, $\hat{\mathbf{L}}$ and $\hat{\mathbf{S}}$ precess with the same angular velocity

$$\Omega_p = \left(2+\frac{3m_2}{2m_1}\right)\frac{J}{r^3} \tag{32}$$

around the fixed direction

$$\hat{\mathbf{J}}_0 = \hat{\mathbf{J}} - \epsilon\hat{\mathbf{J}}\times\hat{\mathbf{L}}\,, \tag{33}$$

where

$$\epsilon \equiv \frac{L}{J}\frac{\dot{L}}{L\Omega_p} \ll 1. \tag{34}$$

The quantities $\mathbf{S}_1\cdot\mathbf{S}_2$, $S = |\mathbf{S}_1 + \mathbf{S}_2|$ and

$$\kappa \equiv \hat{\mathbf{S}}\cdot\hat{\mathbf{L}} \tag{35}$$

are constant during the in-spiral. The phase of the gravitational signal contains an additional contribution, the so-called "Thomas precession phase", given by [33]

$$\delta_p\phi(t) = -\int_t^{t_c}\delta_p\dot{\phi}(t')\,dt'\,, \tag{36}$$

where

$$\delta_p\dot{\phi}(t) = \frac{\hat{\boldsymbol{L}}\cdot\hat{\boldsymbol{N}}}{1-(\hat{\boldsymbol{L}}\cdot\hat{\boldsymbol{N}})^2}\,(\hat{\boldsymbol{L}}\times\hat{\boldsymbol{N}})\cdot\dot{\hat{\boldsymbol{L}}}\,. \tag{37}$$

In analogy with the number of wave cycles, we can introduce here the number of precession cycles $\mathcal{N}_p$ that $\hat{\mathbf{L}}$ and $\hat{\mathbf{S}}$ undergo around $\hat{\mathbf{J}}$ from some initial frequency $f_a$, at time $t_{\rm a}$, to the final coalescence at $t_c$:

$$\mathcal{N}_p = \frac{1}{2\,\pi}\int_{t_a}^{t_c}\Omega_p(t)\,dt\,. \tag{38}$$

TABLE II: The total number of precession cycles $\mathcal{N}_p$ and the precession angular frequency $\Omega_p$ at the beginning and end of LISA observations, for the final year of in-spiral of a binary system at redshift $z = 1$ with $\kappa = \hat{\mathbf{S}} \cdot \hat{\mathbf{L}} = 0.9$ for selected values of the masses and spin magnitude.

| $m_1$ ($M_\odot$) | $m_2$ ($M_\odot$) | $S/M^2$ | $\Omega_p$ at $f_a$ ($\times 10^{-4}$ Hz) | $\Omega_p$ at $f_{\rm isco}$ ($\times 10^{-4}$ Hz) | Number of precession cycles |
|---|---|---|---|---|---|
| $10^7$ | $10^7$ | 0.95 | 0.009 | 1.254 | 11 |
| $10^7$ | $10^7$ | 0.50 | 0.007 | 0.892 | 9 |
| $10^7$ | $10^7$ | 0.10 | 0.005 | 0.579 | 7 |
| $10^7$ | $10^6$ | 0.95 | 0.008 | 1.043 | 11 |
| $10^7$ | $10^6$ | 0.50 | 0.005 | 0.632 | 7 |
| $10^7$ | $10^6$ | 0.10 | 0.003 | 0.272 | 4 |
| $10^7$ | $10^5$ | 0.95 | 0.026 | 0.911 | 34 |
| $10^7$ | $10^5$ | 0.50 | 0.014 | 0.489 | 19 |
| $10^7$ | $10^5$ | 0.10 | 0.003 | 0.114 | 5 |
| $10^7$ | $10^4$ | 0.95 | 0.133 | 0.895 | 127 |
| $10^7$ | $10^4$ | 0.50 | 0.064 | 0.472 | 71 |
| $10^7$ | $10^4$ | 0.10 | 0.012 | 0.096 | 15 |
| $10^6$ | $10^6$ | 0.95 | 0.018 | 12.540 | 25 |
| $10^6$ | $10^6$ | 0.50 | 0.015 | 8.919 | 20 |
| $10^6$ | $10^6$ | 0.10 | 0.013 | 5.788 | 16 |
| $10^6$ | $10^5$ | 0.95 | 0.015 | 10.432 | 23 |
| $10^6$ | $10^5$ | 0.50 | 0.011 | 6.319 | 16 |
| $10^6$ | $10^5$ | 0.10 | 0.007 | 2.716 | 9 |
| $10^6$ | $10^4$ | 0.95 | 0.047 | 9.110 | 74 |
| $10^6$ | $10^4$ | 0.50 | 0.025 | 4.892 | 40 |
| $10^6$ | $10^4$ | 0.10 | 0.007 | 1.144 | 11 |
| $10^5$ | $10^5$ | 0.95 | 0.038 | 125.396 | 54 |
| $10^5$ | $10^5$ | 0.50 | 0.034 | 89.194 | 46 |
| $10^5$ | $10^5$ | 0.10 | 0.030 | 57.877 | 39 |
| $10^5$ | $10^4$ | 0.95 | 0.030 | 104.315 | 48 |
| $10^5$ | $10^4$ | 0.50 | 0.023 | 63.186 | 34 |
| $10^5$ | $10^4$ | 0.10 | 0.016 | 27.159 | 22 |

Depending on the mass ratio of a binary system, whether $m_1 \sim m_2$ ($L \gg S$) or $m_1 \gg m_2$ ($L \ll S$), $\mathcal{N}_p$ is well approximated by the following expressions:

$$\mathcal{N}_p \approx \begin{cases} 10 \left(1 + \frac{3\,m_2}{4\,m_1}\right) \left(\frac{m}{10^6\,M_\odot}\right)^{-1} \left(\frac{f_a}{10^{-4}\,\mathrm{Hz}}\right)^{-1} & (L \gg S) \\ 2 \left(1 + \frac{3\,m_2}{4\,m_1}\right) \left(\frac{m_1}{m_2}\right) \left(\frac{S}{m_1^2}\right) \left(\frac{m}{10^6\,M_\odot}\right)^{-2/3} \left(\frac{f_a}{10^{-4}\,\mathrm{Hz}}\right)^{-2/3} & (L \ll S) \end{cases} . \tag{39}$$

Notice that the precession cycles accumulate at low frequency, and, for $L \gg S$, $\mathcal{N}_p$ does not depend on $S$; if $L \ll S$, $\mathcal{N}_p \propto (m_1/m_2) \gg 1$ which could therefore generate a very large number of precessions. In Table II we show the number of precession cycles $\mathcal{N}_p$ and the value of the precession frequency $\Omega_p$ at $f_a$ and $f_{\rm isco}$ for a number of choices of the mass of a binary system.

Using Eq. (32) we define now the *precession angle* $\alpha$ as

$$\frac{d\alpha}{dt} = \Omega_p \,, \tag{40}$$

From Eqs. (31), (33) and (35) it is straightforward to derive the relevant equations for the evolution of the total and

orbital angular momentum:

$$\hat{\mathbf{J}} = \frac{\hat{\mathbf{L}} + \Upsilon\hat{\mathbf{S}}}{(1 + 2\kappa\,\Upsilon + \Upsilon^2)^{1/2}}\,, \tag{41a}$$

$$J = L\left(1 + 2\,\Upsilon + \Upsilon^2\right)^{1/2}\,, \tag{41b}$$

$$\dot{\hat{\mathbf{J}}} = \dot{\Upsilon}\frac{\hat{\mathbf{S}}(1 + \Sigma\Upsilon) - \hat{\mathbf{L}}(\kappa - \Upsilon)}{(1 + 2\kappa\,\Upsilon + \Upsilon^2)^{3/2}}\,, \tag{41c}$$

$$\dot{\hat{\mathbf{L}}} = \Omega_p\left[\hat{\mathbf{J}}_0 \times \hat{\mathbf{L}} + \epsilon(\hat{\mathbf{J}}_0 \times \hat{\mathbf{L}}) \times \hat{\mathbf{L}}\right]\,, \tag{41d}$$

$$\hat{\mathbf{L}} = \hat{\mathbf{J}}_0 \cos\lambda_L + \frac{\hat{\mathbf{z}} - \hat{\mathbf{J}}_0 \cos\theta_J}{\sin\theta_J} \sin\lambda_L \cos\alpha + (\hat{\mathbf{J}}_0 \times \hat{\mathbf{z}})\frac{\sin\lambda_L \sin\alpha}{\sin\theta_J}\,. \tag{41e}$$

In the previous equation $\theta_J$ and $\phi_J$ are the polar coordinates of $\hat{\mathbf{J}}_0$ in the fixed frame and

$$\lambda_L \equiv \arcsin\frac{|\dot{\hat{L}}|}{\Omega_p} \tag{42}$$

is the angle between $\hat{\mathbf{L}}$ and $\hat{\mathbf{J}}$ (at the first order in $\epsilon$, the approximation in which we are working, $\lambda_L$ coincides with the angle between $\hat{\mathbf{L}}$ and $\hat{\mathbf{J}}_0$) and

$$\Upsilon(t) \equiv \frac{S}{L(t)}\,. \tag{43}$$

From Eqs. (32) and (34) one can write explicitly:

$$\Omega_p = \left(2 + \frac{3m_2}{2m_1}\right)\frac{L}{r^3}\mathcal{G}\,, \tag{44}$$

$$\epsilon = \frac{16}{5}\left(\frac{m}{r}\right)^{3/2}\left[\left(1 + \frac{3m_2}{4m_1}\right)\mathcal{G}^2\right]^{-1}\,, \tag{45}$$

where

$$\mathcal{G}^2(f) \equiv 1 + 2\kappa\Upsilon + \Upsilon^2\,. \tag{46}$$

Eqs. (43), (44), (45) and (46) can be used to integrate Eq. (40):

$$\begin{aligned}\alpha = \alpha_c - \frac{96}{5\mu^3 m^3}\left(1 + \frac{3m_2}{4m_1}\right)\Bigg[&2\,(\mathcal{G}\,L)^3 - 3\kappa\,S\,(L + \kappa\,S)\,\mathcal{G}\,L \\ &-3\,\kappa\,S^3\left(1 - \kappa^2\right)\,\mathrm{arcsinh}\left(\frac{L + \kappa\,S}{S\,(1 - \kappa^2)^{1/2}}\right)\Bigg]\,.\end{aligned} \tag{47}$$

In Eq. (47) the angle $\alpha_c$ is a constant of integration that essentially identifies the position of $\hat{\mathbf{L}}$ and $\hat{\mathbf{S}}$ on the precession cone at the reference time $t_c$. Finally, the frequency evolution of $\lambda_L$ – the angle between $\hat{\mathbf{L}}$ and $\hat{\mathbf{J}}$ changes with time – is given by:

$$\sin\lambda_L = \frac{\Upsilon\left(1 - \kappa^2\right)^{1/2}}{(1 + 2\kappa\,\Upsilon + \Upsilon^2)^{1/2}} = \frac{S\,\left(1 - \kappa^2\right)^{1/2}}{L(f)\mathcal{G}(f)}\,, \tag{48a}$$

$$\cos\lambda_L = \frac{1 + \kappa\,\Upsilon}{(1 + 2\kappa\,\Upsilon + \Upsilon^2)^{1/2}} = \frac{L(f) + \kappa\,S}{L(f)\mathcal{G}(f)}\,. \tag{48b}$$

Notice that at the 1.5PN order, which corresponds to the the post-Newtonian order at which we model the waveform in this paper, the contribution of the spins to the GW phase (23) depends only on the parameter $\beta$. However, if one takes into account the change of orientation of the angular momenta, then the spin-orbit coupling is described by three parameters, say $\alpha_c$, $\kappa$ and $S$, on which $\beta$ depends. In the implementation of the computation of the Fisher information matrix, cf Sec. V, we found convenient to use as independent parameters $\beta$, $\kappa$ and $\alpha_c$.

## IV. THE OBSERVED SIGNAL

We can now derive ready-to-use analytical expressions for the signal measured by LISA at the Michelson detector output, Eq. (7), when the source is an in-spiralling binary system of spinning massive black holes. In this case, due to the relativistic spin-orbit coupling, the binary angular momenta, $\mathbf{L}$, $\mathbf{S}_1$ and $\mathbf{S}_2$, precess, following the equations described in Sec.III B. It is worth spelling out the assumption under which the signal is derived: (i) the binary is in circular orbit; (ii) the waveform is modelled using the restricted post$^{1.5}$-Newtonian approximation (amplitude at the lowest quadrupole Newtonian contribution, and GW phase at the 1.5PN order); (iii) the masses and/or spins are such that the system undergoes "simple precession".

In the most general case the signal depends on 17 parameters: 2 mass parameters, 6 parameters related to the BH spins – the magnitude and orientation of each spin – the orbital eccentricity, the luminosity distance (which is a *direct observable* in GW astronomy), 2 angles identifying the location of the source in the sky, two angles that describe the orientation of the orbital plane, one angle that describes the orientation of the ellipse in the orbital plane, an arbitrary reference time, say the time at coalescence, and the signal phase at that time. In the approximation that we consider here the signal depends on 12 unknown parameters (cf the next section for more details). The key new qualitative feature that we introduce here and that is not present in any of the previous analysis [26, 27, 29, 30] is the change of orientation of the orbital angular momentum during the observation. Unlike the model considered in [27, 29], here we consider only the waves emitted at twice the orbital frequency.

Before providing the explicit expression for $h(t)$, it is worth summarising the key motions and the associated time scales that affect the detector output:

- LISA orbits around the Sun, so that the barycentre of the instrument changes position over the timescale of one sidereal year: this motion Doppler-shifts the incoming gravitational waves, and depends only on the source position in the sky;
- The orientation of the LISA arms changes over the same time scale because the detector precesses around the normal to the Ecliptic: this introduces a phase and amplitude modulation which is due to the time-dependent response of the detector to the two orthogonal polarisations $h_+$ and $h_\times$; this effect depends on both the position and orientation of the source in the sky.
- The binary orbital plane changes orientation in the sky with $\mathbf{L}$ and $\mathbf{S}$ that precess around the total angular momentum $\mathbf{J}$, whose direction is essentially constant. The time scale of precession is longer than the orbital period but much shorter than the LISA rotation time-scale and depends on both the source-detector relative orientation and the binary physical parameters (masses and spins): the incoming GW's are therefore *intrinsically* modulated in amplitude and phase.

We consider first the representation of detector output in the time domain $h^{(\iota)}(t)$; we will then turn to the frequency domain representation $\tilde{h}^{(\iota)}(f)$.

### A. The measured signal in the time domain

In the amplitude-and-phase representation, the signal $h^{(\iota)}(t)$, cf Eq. (7), measured by the $\iota$-th Michelson LISA interferometer and produced by the polarisation amplitudes (18a) and (18b) reads

$$h^{(\iota)}(t) = A(t)\, A_p^{(\iota)}(t)\, \cos\left[\phi(t) + \delta_p\phi(t) + \varphi_p^{(\iota)}(t) + \varphi_D(t)\right] . \tag{49}$$

In the previous expression

$$A_p^{(\iota)}(t) \;=\; \frac{\sqrt{3}}{2}\left\{\left[1+\left(\hat{\mathbf{L}}\cdot\hat{\mathbf{N}}\right)^2\right]^2 F_+^{(\iota)}(t)^2 + 4\left(\hat{\mathbf{L}}\cdot\hat{\mathbf{N}}\right)^2 F_\times^{(\iota)}(t)^2\right\}^{1/2} , \tag{50}$$

$$\varphi_p^{(\iota)}(t) \;=\; \tan^{-1}\left\{\frac{2\left(\hat{\mathbf{L}}\cdot\hat{\mathbf{N}}\right)F_\times^{(\iota)}(t)}{\left[1+\left(\hat{\mathbf{L}}\cdot\hat{\mathbf{N}}\right)^2\right]F_+^{(\iota)}(t)}\right\} \tag{51}$$

are the *polarisation amplitude* and *phase*, respectively;

$$\varphi_D(t) = 2\pi R_\oplus f\, \sin\theta_N \cos(\Phi(t)-\phi_N) \qquad (R_\oplus = 1\,\mathrm{AU}) \tag{52}$$

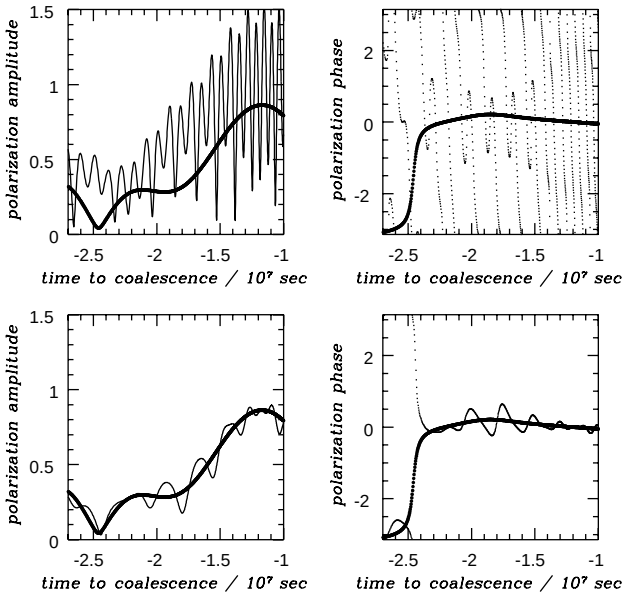


FIG. 1: The evolution of the polarisation amplitude (left panels) and phase (right panels), computed according to Eqs. (50) and (51), for the final year of in-spiral of a binary system as a function of time. The bold solid-line refers to black holes with no spin, the dotted-line (for the phase) and thin solid-line (for the amplitude) to spinning objects. The relevant source parameters are chosen as follows: $m_1 = 10^7\,M_\odot$, $m_2 = 10^5\,M_\odot$, $S/m^2 = 0.95$ and $\hat{\mathbf{S}}\cdot\hat{\mathbf{L}} = 0.5$ (top panels), and $m_1 = m_2 = 10^6\,M_\odot$, $S/m^2 = 0.3$, and $\hat{\mathbf{S}}\cdot\hat{\mathbf{L}} = 0.9$ (bottom panels). The location and initial orientation of the source have been chosen randomly. See the text for further details.

is the *Doppler phase modulation* induced by the motion of the LISA detector around the Sun; $\delta_p\phi(t)$ is the so-called *Thomas precession phase*, Eq. (36), which vanishes for spin-less binary systems; the amplitude of the gravitational wave signal is

$$A[t(f)] = 2\frac{\mathcal{M}^{5/3}}{D}\,[\pi\, f(t)]^{2/3}\,, \tag{53}$$

and the GW phase $\phi(t)$ is given by Eq.(23), where at the 1.5PN order one neglects the term proportional to $(\pi M f)^{4/3}$.

The structure of $h^{(\iota)}(t)$ clearly shows that the signal measured at the detector output is phase and amplitude modulated because of the three effects that we have mentioned above: (ii) the orbital motion of the instrument around the Sun which Doppler-modulates, through $\varphi_D$, the phase of the incoming gravitational wave signal; this effect is the same for $h^{(I)}$ and $h^{(II)}$; (ii) the change of orientation of the detector during the time of observation that through $F_+^{(\iota)}(t)$ and $F_\times^{(\iota)}(t)$ affects $A_p^{(\iota)}$ and $\varphi_p^{(\iota)}$, in different ways depending on $\iota$; (iii) the change of $\hat{\mathbf{L}}$ due to spin-orbit interaction which affects $A_p^{(\iota)}$ and $\varphi_p^{(\iota)}$ through $(\hat{\mathbf{N}}\cdot\hat{\mathbf{L}})$ and $\psi'_N$, cf. Eqs. (8a), (8b), (12), (50) and (51); the impinging signal is *intrinsically* modulated. Furthermore $\delta_p\phi$ adds to the phase of the signal.

In order to complete the analysis of the detector output, we need to provide explicit expressions for $(\hat{\mathbf{L}}\cdot\hat{\mathbf{N}})$, which enters Eq. (50) and (51), and $(\hat{\mathbf{L}}\cdot\hat{\mathbf{z}}')$ and $[\hat{\mathbf{N}}\cdot(\hat{\mathbf{L}}\times\hat{\mathbf{z}}')]$ that are needed to compute $\psi'_N$, Eq. (12), and therefore the

antenna beam patters. Using Eqs. (4) and (41e) we obtain:

$$\begin{aligned}
\hat{\mathbf{L}}\cdot\hat{\mathbf{N}} &= (\hat{\mathbf{J}}_0\cdot\hat{\mathbf{N}})\cos\lambda_L + \frac{\cos\theta_N - (\hat{\mathbf{J}}_0\cdot\hat{\mathbf{N}})\cos\theta_J}{\sin\theta_J}\sin\lambda_L\cos\alpha \\
&\quad + \frac{(\hat{\mathbf{J}}_0\times\hat{\mathbf{z}})\cdot\hat{\mathbf{N}}}{\sin\theta_J}\sin\lambda_L\sin\alpha\,, \qquad (54)\\
\hat{\mathbf{L}}\cdot\hat{\mathbf{z}}' &= (\hat{\mathbf{J}}_0\cdot\hat{\mathbf{z}}')\cos\lambda_L + \frac{1-2\,(\hat{\mathbf{J}}_0\cdot\hat{\mathbf{z}}')\cos\theta_J}{2\sin\theta_J}\sin\lambda_L\cos\alpha \\
&\quad + \frac{(\hat{\mathbf{J}}_0\times\hat{\mathbf{z}})\cdot\hat{\mathbf{z}}'}{\sin\theta_J}\sin\lambda_L\sin\alpha\,, \qquad (55)\\
\hat{\mathbf{N}}\cdot(\hat{\mathbf{L}}\times\hat{\mathbf{z}}') &= \hat{\mathbf{N}}\cdot(\hat{\mathbf{J}}_0\times\hat{\mathbf{z}}')\cos\lambda_L + \frac{\hat{\mathbf{N}}\cdot(\hat{\mathbf{z}}\times\hat{\mathbf{z}}') - \hat{\mathbf{N}}\cdot(\hat{\mathbf{J}}_0\times\hat{\mathbf{z}}')\cos\theta_J}{\sin\theta_J}\sin\lambda_L\cos\alpha \\
&\quad + \frac{\hat{\mathbf{N}}\cdot(\hat{\mathbf{J}}_0\times\hat{\mathbf{z}})\times\hat{\mathbf{z}}'}{\sin\theta_J}\sin\lambda_L\sin\alpha\,. \qquad (56)\\
& \qquad (57)
\end{aligned}$$

In the previous expressions $\sin\lambda_L$, $\cos\lambda_L$ and are $\alpha$ are given by Eqs. (48a), (48b) and (47), respectively, and the remaining quantities describing the orientation of the source with respect of the detector read:

$$\begin{aligned}
\hat{\mathbf{J}}_0\cdot\hat{\mathbf{z}}' &= \frac{1}{2}\cos\theta_J - \frac{\sqrt{3}}{2}\sin\theta_J\cos(\Phi(t)-\phi_J)\,, \qquad (58)\\
\hat{\mathbf{J}}_0\cdot\hat{\mathbf{N}} &= \cos\theta_J\cos\theta_N + \sin\theta_J\sin\theta_N\cos(\phi_J-\phi_N)\,, \qquad (59)\\
\hat{\mathbf{N}}\cdot\left(\hat{\mathbf{J}}_0\times\hat{\mathbf{z}}'\right) &= \frac{1}{2}\sin\theta_N\sin\theta_J\sin(\phi_J-\phi_N) \\
&\quad -\frac{\sqrt{3}}{2}\cos\Phi(t)\left(\cos\theta_J\sin\theta_N\sin\phi_N - \cos\theta_N\sin\theta_J\sin\phi_J\right) \\
&\quad -\frac{\sqrt{3}}{2}\sin\Phi(t)\left(\cos\theta_N\sin\theta_J\cos\phi_J - \cos\theta_J\sin\theta_N\cos\phi_N\right)\,, \qquad (60)\\
\hat{\mathbf{N}}\cdot(\hat{\mathbf{J}}_0\times\hat{\mathbf{z}}) &= \sin\theta_N\sin\theta_J\sin(\phi_J-\phi_N)\,, \qquad (61)\\
\hat{\mathbf{N}}\cdot(\hat{\mathbf{z}}\times\hat{\mathbf{z}}') &= \frac{\sqrt{3}}{2}\,\sin\theta_N\sin\left[\Phi(t)-\phi_N\right]\,, \qquad (62)\\
\hat{\mathbf{J}}\cdot(\hat{\mathbf{z}}\times\hat{\mathbf{z}}') &= \frac{\sqrt{3}}{2}\,\sin\theta_J\sin\left[\Phi(t)-\phi_J\right]\,, \qquad (63)\\
\hat{\mathbf{N}}\cdot(\hat{\mathbf{J}}_0\times\hat{\mathbf{z}})\times\hat{\mathbf{z}}' &= -\frac{1}{2}\sin\theta_J\left[\sqrt{3}\cos\theta_N\cos\left[\Phi(t)-\phi_J\right] + \sin\theta_N\cos(\phi_J-\phi_N)\right]\,. \qquad (64)
\end{aligned}$$

Lastly, we need to compute the scalar and vector products necessary to derive the Thomas precession phase $\delta_p\phi(t)$, Eqs. (36) and (37):

$$(\hat{\boldsymbol{L}}\times\hat{\boldsymbol{N}})\cdot\dot{\hat{L}} = \Omega_p\left[\cos\lambda_L\,(\hat{\mathbf{N}}\cdot\hat{\mathbf{L}}) - (\hat{\mathbf{N}}\cdot\hat{\mathbf{J}}_{\mathbf{0}}) - \epsilon\,\hat{\mathbf{J}}_0\cdot(\hat{\mathbf{L}}\times\hat{\mathbf{N}})\right]\,, \qquad (65)$$

$$\hat{\mathbf{J}}_0\cdot(\hat{\mathbf{L}}\times\hat{\mathbf{N}}) = \frac{\hat{\mathbf{N}}\cdot(\hat{\mathbf{J}}_0\times\hat{\mathbf{z}})}{\sin\theta_J}\sin\lambda_L\cos\alpha + \frac{\cos\theta_J(\hat{\mathbf{N}}\cdot\hat{\mathbf{J}}_0)-\cos\theta_N}{\sin\theta_J}\sin\lambda_L\sin\alpha\,; \qquad (66)$$

$\delta_p\phi(t)$ can be therefore computed using Eqs. (47), (48a), (48b), (54), (58), (59) and (60).

An example of the LISA output when black holes rapidly spin is shown in Figure 1, where we plot the amplitude and phase modulation, Eqs (50) and (51), during the final year of in-spiral. Two cases are actually presented: a binary system with $m_1 = 10^7\,M_\odot$, $m_2 = 10^5\,M_\odot$, $S/m^2 = 0.95$ and $\hat{\mathbf{S}}\cdot\hat{\mathbf{L}} = 0.5$ and an equal mass binary where the parameters correspond to $m_1 = m_2 = 10^6\,M_\odot$, $S/m^2 = 0.3$, and $\hat{\mathbf{S}}\cdot\hat{\mathbf{L}} = 0.9$. The evolution of $A_p(t)$ and $\varphi_p(t)$ for the two sets of physical parameters is compared to the spin-less case. A simple eye inspection shows how dramatic is the effect induced by spins, and it should therefore not come as a surprise the fact that the errors associated to the measurements of the source parameters are strongly affected.

### B. The measured signal in the frequency domain

For several applications in data analysis, it is often more useful to work in the frequency domain, and we will derive now an approximation to the Fourier representation of the signal $h^{(\iota)}(t)$, Eq.(49). Our convention for the Fourier transform $\tilde{g}(f)$ of any real function $g(t)$ is:

$$\tilde{g}(f) = \int_{-\infty}^{\infty} e^{2\pi i f t}\, g(t)\, dt\,. \tag{67}$$

The Fourier transform (67) of the signal $h^{(\iota)}(t)$ can be computed in an rather straightforward way using the stationary phase approximation, see [52], and considering the gravitational waveform $A(t)\cos\phi(t)$ in Eq. (49) as the *carrier signal* modulated by the motion of the detector and the source's orbital plane [26, 33]. Under this assumption, the Fourier transform of the detector output (49) reads:

$$\tilde{h}^{(\iota)}(f) \simeq \begin{cases} \mathcal{A}\, A_p^{(\iota)}[t(f)]\, f^{-7/6}\, e^{\left\{i\left[\Psi(f) - \varphi_p^{(\iota)}[t(f)] - \varphi_D[t(f)] - \delta_p\phi[t(f)]\right]\right\}} & 0 < f \leq f_{\rm isco} \\ 0 & f > f_{\rm isco} \end{cases}, \tag{68}$$

where

$$\mathcal{A} \;=\; \left(\frac{5}{96}\right)^{1/2} \pi^{-2/3}\, \frac{\mathcal{M}^{5/6}}{D} \tag{69}$$

$$\begin{aligned} \Psi(f) \;=\; & 2\pi f t_c - \phi_c - \frac{\pi}{4} + \frac{3}{4}\,(8\pi\mathcal{M}f)^{-5/3}\left[1 + \frac{20}{9}\left(\frac{743}{336} + \frac{11}{4}\,\eta\right)\,(\pi m f)^{2/3}\right. \\ & \left. -4\,(4\pi - \beta)\,(\pi m f) + 10\left(\frac{3058673}{1016064} + \frac{5429}{1008}\,\eta + \frac{617}{144}\,\eta^2 - \sigma\right)\,(\pi m f)^{4/3}\right]. \end{aligned} \tag{70}$$

Notice that in Eq. (70) the term proportional to $(\pi m f)^{4/3}$ correspond to the post$^2$-Newtonian order, and will not be considered in this work.

## V. PARAMETER ESTIMATION

In this section we discuss the errors associated to the parameter measurement when LISA monitors binary systems of rapidly rotating massive black holes in circular orbit. We start by briefly recalling the general concepts and formulae regarding parameter estimation – we refer the reader to [48, 49, 50, 51, 52] and references therein for more details – and then present the results of our analysis applied to LISA data.

### A. Review of signal analysis and parameter estimation

The signal $s(t)$ registered at the detector output is the superposition of noise $n(t)$ and gravitational waves $h(t;\boldsymbol{\lambda})$:

$$s(t) = h(t;\boldsymbol{\lambda}) + n(t)\,; \tag{71}$$

$\boldsymbol{\lambda}$ represents the vector of the unknown parameters (location, masses, spins, etc.) that characterise the actual waveform and that one wishes to estimate from the data stream. We assume the noise to be stationary and Gaussian, characterised by a noise spectral density $S_n(f)$. In the geometrical approach to signal processing it is useful to consider $s(t)$ as a vector in the signal vector space, and to introduce the following inner product between two signals $v$ and $w$ [52]:

$$(v|w) = 2\int_0^{\infty} \frac{\tilde{v}(f)\tilde{w}^*(f) + \tilde{v}^*(f)\tilde{w}(f)}{S_n(f)}\, df\,. \tag{72}$$

According to the definition (72), the optimal signal-to-noise ratio (SNR) at which $h$ can be detected is

$$S/N = \frac{(h|h)}{\mathrm{rms}[(h|n)]} = (h|h)^{1/2}\,. \tag{73}$$

In this paper we discuss the errors associated to the measurement of the unknown parameter vector $\boldsymbol{\lambda}$ that characterises the signal $h(t;\boldsymbol{\lambda})$. In the limit of large SNR, which is clearly the case for LISA observations of massive black hole binary systems, the errors $\Delta\boldsymbol{\lambda}$ follow a Gaussian probability distribution:

$$p(\Delta\boldsymbol{\lambda}) = \left(\frac{\det(\boldsymbol{\Gamma})}{2\,\pi}\right)^{1/2} e^{-\frac{1}{2}\,\Gamma_{jk}\Delta\lambda^j\,\Delta\lambda^k}\,. \tag{74}$$

In Eq.(74) the matrix $\Gamma_{jk}$ is known as the Fisher information matrix, and reads

$$\Gamma^{(\iota)}_{jk} \equiv \left(\frac{\partial h^{(\iota)}}{\partial\lambda^j}\middle|\frac{\partial h^{(\iota)}}{\partial\lambda^k}\right)\,. \tag{75}$$

The *variance-covariance matrix* is simply given by the inverse of the Fisher information matrix:

$$\Sigma^{jk} = \langle\Delta\lambda^j\,\Delta\lambda^k\rangle = \left[\left(\boldsymbol{\Gamma}^{(\iota)}\right)^{-1}\right]^{jk}\,. \tag{76}$$

The matrix $\boldsymbol{\Sigma}$ contains full information about the parameter errors and their correlations, and is what we need to compute (cf next Section) in order to investigate the LISA parameter estimation. In fact the diagonal elements of $\boldsymbol{\Sigma}$ represent the expected mean squared errors

$$\langle(\Delta\lambda^j)^2\rangle = \Sigma^{jj}\,, \tag{77}$$

and its off-diagonal elements provide information about the correlations among different parameters through the correlation coefficients $c^{jk}$:

$$c^{jk} = \frac{\Sigma^{jk}}{\sqrt{\Sigma^{jj}\,\Sigma^{kk}}} \qquad (-1 \le c^{jk} \le +1)\,. \tag{78}$$

In the limit of high signal-to-noise ratio, $\Sigma^{jj}$ provides a tight lower bound to the minimum mean-squared error $\langle(\Delta\lambda^j)^2\rangle$ the so-called Cramer-Rao bound [49, 50]. It is important to notice that the errors (77) and the correlation coefficients (78) depend both on the actual value of the signal parameter vector $\boldsymbol{\lambda}$. For the case of observations with two or more detectors with uncorrelated noise, the Fisher information matrix is simply: $\Gamma_{jk} = \sum_\iota \Gamma^{(\iota)}_{jk}$.

One of the properties that we are interested in is the angular resolution of the instrument, which we define as:

$$\Delta\Omega_N = 2\pi\,\left\{\left\langle\Delta\cos\theta_N^2\right\rangle\,\left\langle\Delta\phi_N^2\right\rangle - \left\langle\Delta\cos\theta_N\,\Delta\phi_N\right\rangle^2\right\}^{1/2}\,; \tag{79}$$

The physical meaning of $\Delta\Omega_N$ is the following: the probability of the source to lie *outside* an (appropriately shaped) error ellipse enclosing a solid angle $\Delta\Omega$ is simply $e^{-\Delta\Omega/\Delta\Omega_N}$.

### B. LISA observations

We discuss now how accurately LISA can measure the source parameters in the case of rapidly spinning black holes. The goal of this section is to investigate whether spins, which have been neglected in studies carried out so far, can significantly affect the estimation of the source parameters. A thorough exploration of this effect requires to probe a very large multi-dimensional parameter space, and it is well outside of the scope of this paper. Here we concentrate on a fiducial source of two $10^6\,M_\odot$ black holes at redshift $z = 1$ – a rather typical LISA source – and we compare the errors associated to the parameter measurements in the case in which spins are present – for large spins, $S/M^2 = 0.95$, and moderate spins $S/M^2 = 0.3$; in both cases $\kappa = 0.9$ – and the case where spins are neglected (the black holes are considered, a priory, to be not spinning).

Before presenting the results we spell out the assumptions under which we compute the errors (77):

- The orbit is circular; we regard such hypothesis as realistic, as we are dealing with massive systems of black holes of comparable mass. As the orbit shrinks due to dynamical friction the eccentricity is likely to decrease [11, 12, 13] and radiation reaction completes the circularisation process before GW's enter the observational window of LISA; in fact the eccentricity $e$ evolves according to $e \propto f^{-19/18}$ [41].

- The black holes are spinning, so that the binary orbit precesses in space. However, in oder to simplify the description of the precession motion, still addressing a realistic astrophysical scenario, we assume that either $m_1 = m_2$ (the case considered in this paper) or $S_2 = 0$ and the spins and angular momentum are not anti-aligned. Under this conditions a binary undergoes the so-called simple precession [33], and the equations describing the evolution of the relevant physical quantities simplify considerably (cf Sec. III B for more details).

- We restrict the analysis only to the in-spiral phase of the whole coalescence. We approximate the waveform $\tilde{h}^{(\iota)}(f;\lambda)$ at the restricted 1.5PN order. The GW signal detected at the LISA output is therefore described by Eqs. (68), (69), and (70). Because we retain terms up to 1.5PN order in the GW phase, in the expression of $\Psi(f)$, Eq. (70), we neglect the last term proportional to $(\pi M f)^{4/3}$. We shut-off the in-spiral waveform at the frequency $f_{\rm isco}$, given by Eq. (15). In the computation of the errors (77) we actually neglect the Thomas precession phase $\delta_p(t)$, Eq. (36). This simplification is motived by computational reasons, and does not affect in any significant way the final results. In fact, $\delta_p[t(f)]$ must be computed numerically at each frequency using the past history of the binary; $\delta_p[t(f)]$ needs then to be included in the integrand of the scalar product( 72) that leads to determination of the elements of the Fisher information matrix. This double numerical integration, which needs to be carried out to high accuracy in order to keep under control numerical instabilities that occur otherwise in the numerical inversion of $\Gamma_{jk}$, makes the computational time very long, due to our limited computational resources. We have checked for a few (random) choices of the source parameters that including $\delta_p[t(f)]$ does not change in any appreciable way the result. This is to be expected. For the physical parameters considered in this paper the Thomas precession phase contribute to $\approx 1$ wave cycle, out of a total $\approx 1500$. It also represents a secular increase in the phase of the GW signal, qualitatively not different from the one given by $\Psi(f)$.

- We consider the fiducial sources to be at redshift $z = 1$ [55]. As the systems are at cosmological distance, the values of all the physical parameters entering the GW signal presented in the previous sections must be considered as the *observed ones*; they differ from the values of the parameters as measured in the source rest frame by a factor $(1+z)$; the parameters are "Doppler-shifted" according to:

$$\begin{aligned} f &\rightarrow \frac{f}{(1+z)}\,, \\ t &\rightarrow (1+z)\,t\,, \\ \mathcal{M} &\rightarrow (1+z)\,\mathcal{M}\,, \\ m &\rightarrow (1+z)\,m\,, \\ \mu &\rightarrow (1+z)\,\mu\,. \end{aligned} \tag{80}$$

- We assume that the instrument observes the whole final year of in-spiral; the GW's sweep therefore the frequency band between the *arrival frequency* $f_{\rm a}$ and the final cut-off frequency $f_{\rm isco}$; $f_{\rm a}$ is determined so that after 1 yr, as measured by an observer in our solar system, the GW instantaneous frequency reaches $f_{\rm isco}$:

$$\begin{aligned} T_{\rm obs} &= t(f_{\rm isco}) - t(f_{\rm a}) \\ &= 1\,{\rm yr} = 3.1556926 \times 10^7\,{\rm sec} \end{aligned} \tag{81}$$

  The range $f_{\rm a} \leq f \leq f_{\rm isco}$ determines the integration domain in (75); values of $f_{\rm a}$ and $f_{\rm isco}$ for selected choices of the source parameters are given in Table I. Note that we do not impose a low-frequency cut-off to LISA; this choice is based on the fact that the real low frequency noise wall of space-based instruments is not very well understood at the moment, placed somewhere in the range $10^{-5}$ Hz - $10^{-4}$ Hz.

- The total noise that affects the observations is given by the superposition of instrumental sources and astrophysical foregrounds of unresolved radiation due to (mainly) galactic white dwarf binary systems [53, 54], the so-called "confusion noise". The total noise spectral density $S_n(f)$ is therefore the sum of these two components, and we use the analytical approximations given in [26, 55] .

- Out of the 17 parameters on which the most general waveform depends, the signal $\tilde{h}^{(\iota)}(f;\lambda)$ that we consider here depends on 12 independent parameters. In our analysis we adopt the following choice of independent parameters: $\ln\mathcal{M}$ and $\ln\mu$ (mass parameters), $\cos\theta_N$, $\phi_N$, $\cos\theta_J$, $\phi_J$, and $\alpha_c$ (geometry of the binary with respect to the detector), $\kappa$ and $\beta$ (spin parameters), $\ln D_L$ (distance of the source) and finally $t_c$ and $\phi_c$.

- We compute the expected mean square errors $\left(\langle\Delta\lambda_j^2\rangle\right)^{1/2}$ and the angular resolution $\Delta\Omega_N$ for the case of observations carried out with one detector and with combined observations of both detectors $I$ and $II$. The

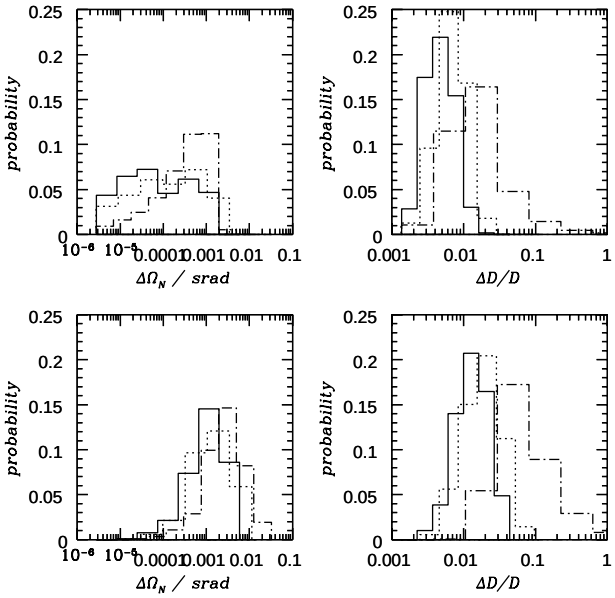


FIG. 2: The probability distribution of $\Delta\Omega_N$ (left) and $\Delta D_L/D_L$ (right), for observations of the final year of in-spiral of a binary system with $m_1 = m_2 = 10^6\, M_\odot$ at $z = 1$. The histograms show the result of a Monte-Carlo simulation, where 1000 sources have been randomly located and oriented in the sky. The bottom panels refer to measurements carried out with only one detector, whereas the top panels describe the results obtained by combining the two independent data streams. The plots compare the errors for different values of the BH spins: $S/m^2 = 0.9$ (solid line), 0.3 (dotted line), and 0 (dotted-dashed line).

analysis is done in the the frequency domain: we first compute analytically the derivatives $\partial h^{(\iota)}/\partial\lambda^j$, where $j = 1, .., 12$, then compute numerically $\Gamma_{jk}$ and $\Sigma^{jk}$, Eqs. (75) and (76); the integration and matrix inversion are performed using numerical routines of the NAG library.

LISA parameter estimation strongly depends (the results vary by orders of magnitude) on the actual value of the signal parameters. In particular, one of the key set of parameters that affect the errors is the location and orientation of a source with respect to the detector. This represents already a large parameter space that one needs to explore in order to obtain meaningful results. We perform this exploration by means of Monte-Carlo simulations, which therefore affect the way in which the results are presented, given in terms of probability distributions. For each set of physical parameters, we select randomly the 5 geometrical parameters ($\theta_N$, $\phi_N$, $\theta_J$, $\phi_J$ and $\alpha_c$) from a uniform distribution in $\cos\theta_N$, $\phi_N$, $\cos\theta_J$, $\phi_J$ and $\alpha_c$. The Monte-Carlo simulation is done on 1000 different sets of angles. As far as the other 7 parameters are concerned we chose them as follows. We consider a fiducial source at redshift $z = 1$, with $m_1 = m_2 = 10^6\, M_\odot$ (which sets the 3 parameters $D_L$, $\mathcal{M}$ and $\mu$), with $t_c = \phi_c = 0$. We fix the *tilt angle* parameter $\kappa = 0.9$, and we explore three different values of the size of the spin $S$: (i) $S/M^2 = 0.95$, (ii) $S/M^2 = 0.3$ and (iii) $S = 0$. Notice that given $m_1$, $m_2$, $S$ and $\kappa$ we can easily derive $\beta$. It is worth noticing that in this paper we do not explore the effect of the tilt angle $\cos^{-1}\kappa$, which is also likely to affect the errors. Such analysis is currently in progress [37]. We would also like to stress that for the case $S = 0$ the waveform that we actually consider is the one corresponding to the non-precessing restricted 2PN approximation (this is the waveform used in [30], very similar to the one used in [26], which is the non-precessing restricted 1.5PN approximation). This is equivalent to assuming that we know *a priori* that spins are zero and the binary system does no precess. Note that this is different from estimating the source parameters using the waveform (68) where precession is included, and assuming $S \ll 1$. In the case $S = 0$ we need to estimate only 11 parameters, and not 12. The reason of this choice is to compare existing results in the literature with our new ones that take into account spin-orbit modulations.

Figs 2, 3 and 4 summarise the key results. Figs 2, 3 show the probability distribution of the parameter errors, for $\Delta\Omega_N$, $\Delta D_L/D_L$, $\Delta\mathcal{M}/\mathcal{M}$ and $\Delta\mu/\mu$. Fig 4 shows the cumulative probability distributions: if we define $\xi \equiv \Delta\lambda^j$, the plots show $P(\xi < \xi_0) = \int_0^{\xi_0} p(\xi')d\xi'$ as a function of $\xi_0$. Each plot compares the non-spinning case with the cases

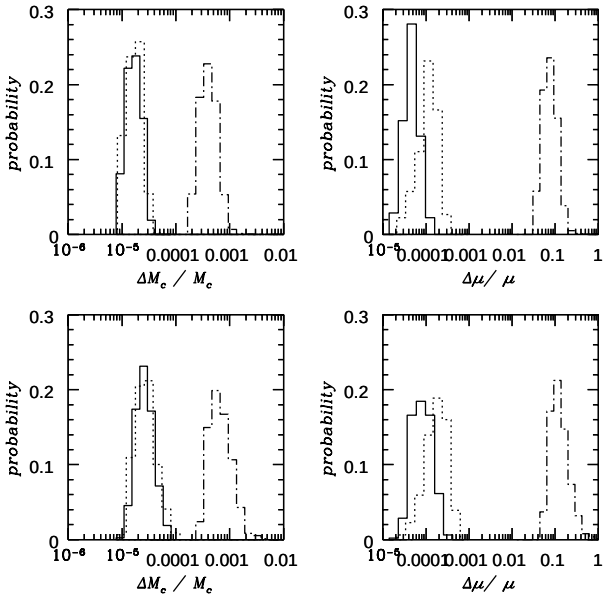


FIG. 3: The probability distribution of $\Delta\mathcal{M}/\mathcal{M}$ (left) and $\Delta\mu/\mu$ (right) for observations carried out with only one interferometer (bottom) and the two combined LISA outputs (top). The parameters are the same as in Fig 2.

in which the black holes are spinning with two different value of the spins, $S/M^2 = 0.95$ and 0.3 .

The key result, which is absolutely clear from Figs 2, 3 and 4 is that the errors in the spinning-case are smaller than in the non-spinning one, even if the number of parameters that one needs to estimate is greater (12 instead of 11). One can intuitively understand this behaviour by looking at Figure 1, which shows the amplitude and phase evolution of the signal recorded at the LISA output: precessing binaries show a much greater richness of features than non-spinning sources. These are the features that help in measuring the parameters.

However, despite all the parameters are estimated with smaller errors with respect to the non-spinning case, there is striking difference between the "position parameters" – location in the sky and luminosity distance – and mass parameters. In fact, the errors $\Delta\Omega_N$ and $\Delta D_L/D_L$ are reduced by a factor 2-to-10 depending on the actual value of the source parameter. We know that LISA reconstruct the position of the source in the sky by exploiting the modulation in the amplitude and phase of the signal, and precession introduces one additional modulation effect which can improve the determination of $\hat{\mathbf{N}}$ and de-correlates $D_L$ from $\mathcal{M}$, which improves the measurement of the luminosity distance. Still, the change of position and orientation of LISA is the main effect that allows the source to be located. The improvement in $\Delta\Omega_N$ and $\Delta D_L/D_L$ is however significant: the fraction of sources that can be located within, say, one square degree is 10% for non-spinning binaries, 35% for binaries with 0.3 and 50% with 0.95 (for $\kappa = 0.9$). The systems whose distance is known to better than 1% is about 60% for non-spinning binaries, and essentially the totality for spinning binaries.

The situation is radically different for the masses: in the non-spinning case the instrument reconstructs the value of the two mass parameters by staying in phase with the GW phase, whose time evolution is mainly controlled by $\mathcal{M}$ (the leading Newtonian term) and, to a less extent, by $\mu$, through the post-Newtonian corrections, cf Eqs. (23), (70) and Table I. $\mathcal{M}$ and $\mu$ play no role in the amplitude and phase modulation, $A_p(t)$ and $\varphi_p(t)$, Eqs (50) and (51). As a consequence, $\mathcal{M}$ is measured much more accurately, by a factor $\sim 100$ or more, than $\mu$, see Fig (3) and [26, 30]. If spins are present, the masses start to play a role also in $A_p(t)$ and $\varphi_p(t)$, because they control the rate at which $\mathbf{L}$ and $\mathbf{S}$ precess, and therefore are responsible for the intrinsic amplitude and phase modulation of the signal. This has two effects on the parameter estimation: it de-correlates $\mathcal{M}$ from $\mu$ (at the Newtonian order the two mass parameters are even degenerate) and provides new features in the measured signal that improve the parameter estimation. The net effect is that the errors in $\mathcal{M}$ and $\mu$ are now of the same order, with a drastic improvement with respect to the non-spinning case, of by a factor $\sim 50$ and $\sim 10^3$ for $\Delta\mathcal{M}/\mathcal{M}$ and $\Delta\mu/\mu$, respectively; $\Delta\mathcal{M}/\mathcal{M}$ is still $\approx 3$ times smaller than $\Delta\mu/\mu$, due to the role played by $\mathcal{M}$ in the GW phase $\phi(t)$. It also clear that the additional signature

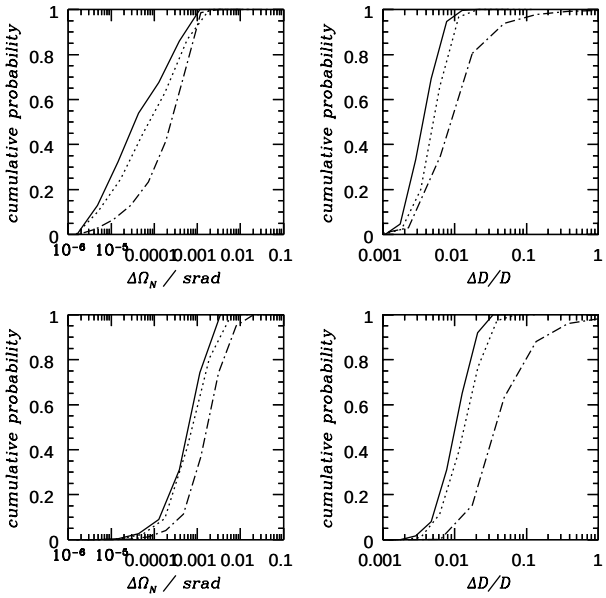


FIG. 4: Same as Figure 2, but now the cumulative probability distributions as a function of the parameters $\Delta\Omega_N$ and $\Delta D_L/D_L$ are shown. See text for more details

produced by the masses on the amplitude and phase modulation helps in removing the correlation between $\mathcal{M}$ and $D_L$, therefore reducing $\Delta D_L/D_L$, as we have already mentioned.

To summarise, the parameters of two $10^6\,M_\odot$ black holes spiralling toward the final merger at $z = 1$, and rapidly rotating, say $S/M^2 = 0.95$ and $\kappa = 0.9$, can be measured very accurately: $\mathcal{M}$ and $\mu$ can be measured to a few parts in $10^5$, the luminosity distance to better than 1% (in some cases almost 0.1%), and with an error box in the sky $10^{-6}\,\mathrm{srad} \lesssim \Delta\Omega_N \sim 10^{-3}\,\mathrm{srad}$. Notice that the errors scale with the distance roughly as $\Delta\Omega_N \sim 1/D_L^2$ and $\Delta\mathcal{M}/\mathcal{M} \sim \Delta\mu/\mu \sim \Delta D_L/D_L \sim 1/D_L$. This would be strictly true for white noise, which is not the case for LISA. In particular going to higher redshift, one can expect a degradation of the measurements more severe than the one predicted by this simple scaling, because GW's are red-shifted to lower frequencies where the noise is higher and some initial portion of the signal falls out of the observational window.

For multi-band, electro-magnetic and gravitational, observations of the same event the key parameter is the instrument's angular resolution. In fact there is some hope that LISA will have enough angular resolution to locate the galaxy or galaxy cluster where a coalescence of massive black holes takes place; this would enable other telescopes to be pointed at the same area of the sky and to observe the aftermath of such catastrophic event. However, previous studies [26, 27, 29, 30] have concluded that this might actually be impossible for sources at $z \approx 1$ (or beyond), because of the poor angular resolution of GW observations. In short, the results of our analysis suggest that in some exceptional case LISA might be able to identify the host galaxy cluster of a MBH binary of $10^6 M_\odot$ at $z = 1$, but in general the LISA error box will contain several hundreds of galaxy clusters and $\gtrsim 10^5$ galaxies, all of them potential hosts of a LISA detected source. Such conclusion can be easily derived by comparing the LISA angular resolution with the one of other telescopes and the angular size of galaxies at high redshift. An optical telescope, such as the Keck telescope, has a field of view of about 1 square degree. Chandra has a square field of view of $16 \times 16$ arcmin with a spatial resolution of $\simeq 1$ arcsec, and XMM has a circular field of view with radius 15 arcmin and a spatial resolution of a few arcsec. INTEGRAL has an even wider circular field of view – the radius is 10 degree – with a poorer spatial resolution (12 arcmin). There is therefore no doubt that, for a typical LISA source at $z = 1$, GW observations will provide information accurate enough to cover the interesting portion of the sky with a single observation by one of (or all) the former instruments. At $z = 1$, the typical size of a galaxy is $\simeq 3$ arcsec and the typical size of a galaxy cluster is $\simeq 2$ arcmin. In a very few lucky occasions LISA will be able to detect a source with $\Delta\Omega_N \approx 3 \times 10^{-3}\,\mathrm{deg}^2$, but more typically the angular resolution is $\Delta\Omega_N \approx 0.3\,\mathrm{deg}^2$, and could be much worse for a few detections ($\Delta\Omega_N \approx 5\,\mathrm{deg}^2$). It is therefore clear that for the "high spatial resolution" GW detections, only $\approx 3$ galaxy clusters will fall in the LISA

error box, but more typically the number of clusters will be $\approx 300$. If there is still a small (but not negligible) chance of identifying the galaxy cluster hosting a GW source, the chances of pin-pointing the host galaxy seem to be very bleak (the former numbers need to be multiplied by a factor $\sim 10^3$ for galaxies).

## VI. CONCLUSION

We have considered LISA observations of massive black hole binary systems in the final stage of in-spiral for rapidly rotating black holes. We have restricted our analysis to comparable mass objects in circular orbit, modelling the radiation at the restricted post$^{1.5}$-Newtonian order assuming simple precession. We have derived read-to-use analytical expressions for the signal registered at the detector output, both in the time and frequency domain, and have determined the mean-square-errors associated to the parameter measurements for equal mass $10^6 M_\odot$ binary systems at $z = 1$ for selected spin parameters and a wide range of source locations and orientations. Our analysis clearly shows that the presence of spins reduces (by orders of magnitude, for some parameters) the errors with which the source parameters are measured. LISA is therefore a more powerful telescope than previously thought if spins play a significant role. The main shortcoming of our analysis is the limited region of the parameter space that we have been able to explore, which is entirely due to our limited computational resources. Such analysis is currently in progress [37]. Of particular interest is the exploration of the parameter space in the case where the masses are not comparable, *i.e.* the mass ratio is $\sim 0.1$ or smaller. Our present understanding of the relevant astrophysical scenarios suggests, in fact, that the formation of unequal mass binaries should be regarded as the rule rather than the exception. When the mass ratio increases, the number of precession cycles detected at the LISA output will increase as well, cf. Table II and Eq. (39). It is therefore conceivable that precession will be even more effective in breaking the degeneracy among the parameters, in particular the two masses. However the amount of intrinsic rotation $S$ shall also play a crucial role, as the number of precession cycles is proportional to $S$. Preliminary results suggest that for $m_2/m_1 = 0.1$ and rapidly rotating systems ($S/M^2 \approx 0.9$) the estimation of the mass parameters and the angular resolution improve by a factor of a few, with respect to the equal mass case, provided that the signal-to-noise ratio is not strongly affected. In general, in fact, unequal mass systems will be detected at a lower SNR, so that precession compensates for the loss of SNR. The latter eventually dominates the effect of rotation when $m_2/m_1$ decreases further and compromises the accuracy with which parameters can be measured.

### Acknowledgments

We would like to thank C. Cutler and A. Sintes for several discussions about LISA parameter estimation. We would also like to thank L. Jones and I. Stevens for discussions about high-redshift surveys of galaxies and clusters.

[1] P. L. Bender et al., *LISA Pre-Phase A Report; Second Edition*, MPQ 233 (1998). P. L. Bender et al., *LISA – System and Technology Study Report*, ESA-SCI(2000)11, (2000). http://www.lisa.jpl.gov
[2] C. Cutler and K. S. Thorne, *An Overview of Gravitational-Wave Sources*, to appear in Proceedings of GR16 (Durban, South Africa, 2001), gr-qc/0204090.
[3] J. Magorrian et al, AJ **115**, 2285 (1998).
[4] D. Richstone et al., Nature **395**, A14 (1998).
[5] R. Genzel, A. Eckart, T. Ott, and F. Eisenhauer, Mont. Not. Roy. Astron. Soc. **291**, 219 (1997).
[6] M. Miyoshi, J. Moran, J. Herrnstein, L. Greenhill, N. Nakai, P. Diamond, M. and Inoue, Nature **373**, 127 (1995).
[7] E. Maoz, Astrophys. J. **494**, L181 (1998).
[8] X. Fan et al, AJ **122**, 2833 (2001).
[9] J. S. B. Wyithe and A. Loeb, astro-ph/0206154.
[10] D. Merritt and L. Ferrarese, ApJ **547**, 140 (2001).
[11] M. C. Begelman, R. D. Blandford, and M. J. Rees, Nature **287**, 307 (1980).
[12] A. Vecchio, M. Colpi and A. Polnarev, ApJ **433**, 733 (1994)
[13] M. Rajagopar and R. W. Romani, ApJ **446**, 543 (1995).
[14] M. Milosavljevic and D. Merritt, ApJ **563**, 34 (2001).
[15] Q. Yu, MNRAS **331**, 935 (2002).
[16] A. Gould and H. Rix, ApJ **532**, L29 (2000)
[17] P. J. Armitage and P. Natarajan, ApJ **567**, L9 (2002)
[18] M. G. Haehnelt, Mont. Not. Roy. Astron. Soc. **269**, 199 (1994).

[19] M. G. Haehnelt, in *Laser Interferometer Space Antenna*, ed. W. M. Falkner (AIP Conference Proceedings 456), pp. 45-49 (1998).
[20] A. Vecchio, Class. Quant. Grav. **14**, 1431 (1997).
[21] K. Menou, Z. Haiman and V. K. Narayanan. ApJ **558**, 535 (2001)
[22] K. Menou 2002, astro-ph/0301397
[23] A. H. Jaffe and D. C. Backer, astro-ph/0210148 (2002).
[24] J. S. B. Wyithe and A. Loeb, astro-ph/0211556.
[25] T. Pursimo et al, Astron. Astrophys. Suppl **146**, 141 (2000).
[26] C. Cutler, Phys. Rev. D **57**, 7089 (1998).
[27] A. M. Sintes and A.Vecchio, in *Gravitational Waves – Third Amaldi Conference*, Ed. S. Meshkov (American Institute of Physics), pp. 403-404 (2000).
[28] A. M. Sintes at al, in preparation
[29] T. A Moore and R. W. Hellings, R. W., Phys. Rev D. **65**, 062001 (2001).
[30] S. Hughes, MNRAS **331**, 805 (2002)
[31] N. Seto, PRD in press.
[32] S. A. Hughes and R. D. Blandford, Ap.J. Lett (in press), astro-ph/0208484
[33] T. A. Apostolatos, C. Cutler, G. S. Sussman and K. S. Thorne Phys. Rev. D **49**, 6274 (1994).
[34] L.E. Kidder, Phys. Rev. D **52**, 821 (1995).
[35] A. Vecchio and C. Cutler, in *Laser Interferometer Space Antenna*, ed. W. M. Falkner (AIP Conference Proceedings 456), pp. 101-109 (1998).
[36] A. Vecchio, in *Gravitational Waves – Third Amaldi Conference*, Ed. S. Meshkov (American Institute of Physics), pp. 238-247 (2000).
[37] A. Vecchio et al, in preparation.
[38] We would like to caution the reader of the different notation used in this paper with respect to [26]: the reference frames $(x, y, z)$ and $(x', y', z')$ of this paper coincide, respectively, with the frames $(\bar{x}, \bar{y}, \bar{z})$ and $(x, y, z)$ of [26].
[39] L. Blanchet, Living Review in Relativity 2002-3 http://www.livingreviews.org/Articles/Volume5/2002-3blanchet/index.html (2002)
[40] E. E. Flanagan and S. Hughes, Phys. Rev. D **57**, 4535, 1998.
[41] P. C. Peters, Phys. Rev. **136**, B1224 (1964).
[42] K.S. Thorne, in *300 Years of Gravitation*, edited by S. W. Hawking and W. Israel (Cambridge University Press, Cambridge, England, 1987), pp. 330-458.
[43] L. Blanchet, B.R. Iyer, C.M. Will and A.G. Wiseman, Class. Quantum. Gr. **13**, 575, (1996).
[44] S. Weinberg *Gravitation and Cosmology: Principles and Applications of the General Theory of Relativity* (New York: Wiley) (1972)
[45] L. Blanchet, T. Damour, B.R. Iyer, C.M. Will and A.G. Wiseman, Phys. Rev. Lett. **74**, 3515 (1995).
[46] B. M. Barker and R. F. O'Connell, Phys. Rev. D **12**, 329 (1975).
[47] K.S. Thorne and J. B. Hartle, Phys. Rev. D **31**, 1815 (1985).
[48] L. A. Wainstein and V. D.Zubakov, *Extraction of signals from noise*, Dover, New York (1962).
[49] C.W. Helstrom, *Statistical Theory of Signal Detection*, 2nd edition, Pergamon Press, London (1968).
[50] D. Nicholson and A. Vecchio, Phys. Rev. D **57**, 4588 (1998).
[51] L. S. Finn, Phys. Rev. D **46**, 5236 (1992).
[52] C. Cutler and E.E. Flanagan, Phys. Rev. D **49**, 2658 (1994)
[53] D. Hils, P. L. Bender, and R. F. Webbink, Ap. J. **360**, 75 (1990).
[54] P. L. Bender and D. Hils, Class. and Quantum Grav. **14**, 1439 (1997).
[55] In this paper we are mainly concerned with a comparison of the errors obtained without considering spins with the ones that are given when spins are included in the signal. It is therefore clear that the actual redshift (distance) of the fiducial source and the choice of the expected noise spectral density (instrumetal noise and confusion noise) have little interest, as far as the same values are used in the two cases.